

Metal-Organic Frameworks and Nanomaterials for Oxygen Evolution Reaction



Thesis Submitted for the Degree of

Doctor of Philosophy

By

Shweta Pal

Supervisor

Prof. Rajiv Prakash

**SCHOOL OF MATERIALS SCIENCE & TECHNOLOGY
INDIAN INSTITUTE OF TECHNOLOGY
(BANARAS HINDU UNIVERSITY)
VARANASI-221005**

Roll. No. 17111014

2022

Acknowledgement

The work presented in this thesis would not have been possible without my close association with many peoples who were always there when I needed them the most. I take this opportunity to acknowledge them and extend my sincere gratitude for helping me make this thesis a possibility. At this moment of accomplishment, first of all, I would like to pay homage to the founder of Banaras Hindu University, Pandit Madan Mohan Malvia ji, who made this glorious temple to realize spiritual, technical, and scientific knowledge about this vast existing universe.

*I embrace the opportunity to express my deep sense of gratitude to my supervisor **Dr. Rajiv Prakash**, Professor, School of Materials Science & Technology, IIT (B.H.U.), Varanasi, (now Director, IIT Bhilai, Raipur, Chattisgarh) for his constant guidance, valuable suggestions, and kind encouragement during my association with his research group. His encouragement, constant support, intellectual stimulation, perceptive guidance, immensely valuable ideas, and suggestions from the initial to the final level enabled me to develop an understanding of the subject. His scholarly suggestions, prudent admonitions, immense interest, constant help, and affectionate behaviour have been a source of inspiration for me. His suggestions will remain with me as an inexhaustible source of scientific learning throughout my life.*

*I would like to express my sincere and whole-hearted gratitude to **Prof. Dhananjay Pandey, Prof. Jitendra Kumar, Prof. Pralay Maiti, Dr. S. R. Singh, Dr. Chandan Upadhyay, Dr. Chandana Rath, Dr. Akhilesh Kumar Singh, Dr. Bola Nath Pal, Dr. Ashish Kumar Mishra, Dr. Sanjay Singh, Dr. Shravan kumar Mishra and Dr. Nikhil Kumar, Dr. Ravi Panwar** (School of Materials Science and Technology, IIT-BHU, Varanasi) for discussion during seminars and valuable suggestions given by them and **Dr. Nand Kishore Prasad** (Metallurgical Engineering Department) for using his lab furnace. I am indeed obliged and sincerely thankful to my RPEC member **Dr. Indrajit Sinha**, Department of Chemistry, IIT- BHU, for his guidance and untiring attention right from the inception to the successful completion of assigned research work. I am thankful to the unknown reviewers who have rejected my papers several times in some of the*

Acknowledgement

international conferences and journals. The comments that they provided helped to polish our articles in better shape. But the bigger and nobler cause of thanking them is that the rejections have equipped me with a high level of patience and helped me a lot to exercise/implement my spiritual thoughts in practice.

*My acknowledgement will never be complete without the special mention of my lab seniors who have taught me the lab culture and have lived by example to make me understand the hard facts of life. I would like to acknowledge **Dr. Narsingh Raw Nirala, Dr. Uday Pratap Azad, Dr. Monika Srivastava, Dr. Ashish Kumar, Dr. Ashish Kumar Singh, Dr. Rajiv Kumar Pandey, Dr. Gopal Ji, Dr. Neeraj Giri, Dr. Madhu Tiwari, Dr. Kashish, Dr. Preeti Tiwari, Dr. Manish Kumar Singh, Dr. Richa Mishra, Dr. Vinita, Dr. Chandrajeet Verma, Dr. Annirudha Jaiswal, Vineet Kumar Mall, Dr. Ravi Prakash Ojha, Dr. Nikhil and Dr. Ajay Kumar** for all their support and motivation during the initial days of my PhD. I can see my thesis in the good shape because of his help in formatting the entire thesis. I express my special thanks to **Dr. Ashish Kumar and Dr. Uday Pratap Azad** for his guidance, support, motivation and valuable suggestions.*

*Also, I am thankful to my lab fellows and juniors of my lab specially **Dr. Subhajit, Dr. Priya, Shivam, Saurabh, Radhe, Rajpal, Shipra, Nupur, Preetam and Gaurav** for their helping behavior. It's my fortune to gratefully acknowledge to my research seniors and fellows from the Materials Science, **Dr. Neela Pal, Dr. Bishnu Pada Majee, Pooja, Krishna, Dr. Shanu, Manish, Dr. Shivam and Abahy.** Also from the Department of Chemistry, **Dr. Shaili Pal, Dr. Daraksha Hussain, Dr. Jyoti Kuntal** and from the Department of Physics, **Dr. Kanchan Yadav.** I am also thankful to my dear friends, **Dr. Aarti, Dr. Priya, Dr. Subhajit, Dr. Arshala, Dr. Jyoti, Dr. Anjali, Dr. Shubham, Dr. Ashvani, Dr. Asish, Dr. Surendra** and to whom I could not mention here who helped me directly or indirectly throughout the work. I am thankful to all non-teaching staff of SMST, IIT (BHU) and all CIFC (Central Instrumental Facility Centre) members for their cooperation at all levels. I express my indebtedness to my Bade Papa **Sri. Awadhesh Kumar Pal** and Badi Mammi **Smt. Abhilasha Pal** and my parents **Sri. Dinesh Kumar Pal and Smt. Shashi Pal.** Also,*

Acknowledgement

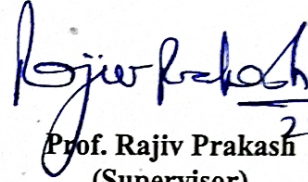
I express my gratitude to my sisters Dr. Archana Pal, Dr. Shaili Pal, Sonam Pal, Akanksha Pal, Janki Pal; brothers Dr. Saurabh Pal, Dr. Suryansh Chandra, Siddhatant Chandra, Sarthak Pal, Ansh Pal, Reyansh Pal, Dr. Kumar Ramesh (jija ji), and sweet little boy of my family 'Advik Kumar' for their love, affection and support during every moment of my life. This work would not have been possible without the grace of the "Lord Shiva and Mata Di."

(Shweta Pal)

CERTIFICATE

It is certified that the work contained in the thesis titled "Metal-organic framework and nanomaterials for oxygen evolution reaction" by "Shweta Pal" has been carried out under my supervision and this work has not been submitted elsewhere for a degree.

It is further certified that the student has fulfilled all the requirements of Comprehensive, Candidacy, and SOTA.



Prof. Rajiv Prakash
(Supervisor)

School of Materials Science &
Technology,
Indian Institute of Technology,
Banaras Hindu University,
Varanasi-221005

Professor/आचार्य

School of Materials Science & Technology/पदार्थ विज्ञान एवं प्रौद्योगिकी स्कूल
Indian Institute of Technology/भारतीय प्रौद्योगिकी संस्थान
(Banaras Hindu University), Varanasi/काशी हिन्दू विश्वविद्यालय, वाराणसी

DECLARATION BY THE CANDIDATE

I, *Shweta Pal* certify that the work embodied in this thesis is my own bonafide work and carried out by me under the supervision of *Prof. Rajiv Prakash* from July 2017 to July 2022 at the *School of Materials Science & Technology*, Indian Institute of Technology, Banaras Hindu University, Varanasi. The matter embodied in this thesis has not been submitted for the award of any other degree/diploma. I declare that I have faithfully acknowledged and given credits to the research workers wherever their works have been cited in my work in this thesis. I further declare that I have not willfully copied any other's work, paragraphs, text, data, results, etc., reported in journals, books, magazines, reports, dissertations, theses, etc., or available at websites and have not included them in this thesis and have not cited as my own work.

Date:

Place: IIT (BHU), Varanasi

Shweta Pal
(Shweta Pal)

Certificate by the Supervisor

It is certified that the above statement made by the student is correct to the best of my knowledge.

Rajiv Prakash
Professor/आचार्य 25/11/2022
School of Materials Science & Technology
Indian Institute of Technology
Banaras Hindu University, Varanasi
कोशी हिन्दू विश्वविद्यालय, वाराणसी

Chintan
Coordinator 01/12/22

School of Materials Science & Technology,
IIT (BHU), Varanasi

Coordinator/समन्वयक

School of Materials Science & Technology/पदार्थ विज्ञान एवं प्रौद्योगिकी स्कूल
Indian Institute of Technology/भारतीय प्रौद्योगिकी संस्थान
(Banaras Hindu University), Varanasi/काशी हिन्दू विश्वविद्यालय, वाराणसी

COPYRIGHT TRANSFER CERTIFICATE

Title of the Thesis: Metal-organic framework and nanomaterials for oxygen evolution reaction

Name of the Student: Shweta Pal

Copyright Transfer


The undersigned hereby assigns to the Indian Institute of Technology (Banaras Hindu University) Varanasi all rights under copyright that may exist in and for the above thesis submitted for the award of the "*Doctor of Philosophy*".

Date:

Place: IIT (BHU), Varanasi

Shweta Pal
(Shweta Pal)

Note: However, the author may reproduce or authorize others to reproduce material extracted verbatim from the thesis or derivative of the thesis for the author's personal use, provided that the source and the Institute's copyright notice are indicated.



*Dedicated to
My
Grandparents*

"Be Alive, Be Joyful, Be Trust on yourself.
Be passionate about your work".

List of Abbreviations

kWh	:	Kilowatt-hours
BkWh	:	Billion kilowatt hours
RES	:	Renewable energy sources
HER	:	Hydrogen evolution reaction
OER	:	Oxygen evolution reaction
ORR	:	Oxygen reduction reaction
ECS	:	Energy conversion and storage devices
LDH	:	Layered double hydroxide
TMCs	:	Transition metal-chalcogenides
MOFs	:	Metal-organic frameworks
η	:	Overpotential
b	:	Tafel slope
ECSA	:	Electroactive surface area
CA	:	Chronoamperometry
ZnDTO	:	Zincdithioamide
Ni-Fe-PBA-NC	:	Nickel-iron-Prussian blue analogue nanocube
NSC	:	N/S/Zn-doped porous carbon
AA	:	Anthranilic Acid
DMF	:	Dimethylformamide
μL	:	Microliter
GCE	:	Glassy carbon electrode
UV-Vis	:	Ultraviolet-visible
FT-IR	:	Fourier transform infrared
XRD	:	X-ray diffraction
FE-SEM	:	Field emission scanning electron microscopy
XPS	:	X-ray photoelectron spectroscopy

List of Abbreviations

BET	:	Brunauer–Emmett–Teller
TGA	:	Thermogravimetric analysis
CV	:	Cyclic voltammetry
LSV	:	Linear sweep voltammetry
EIS	:	Electrochemical impedance spectroscopy
R_{ct}	:	Charge-transfer resistance
R_{so}	:	Solution resistance
QPE	:	Constant phase element
RHE	:	Reversible hydrogen electrode
DTO	:	Dithioamide
RuO_2	:	Ruthenium oxide
Co_3O_4	:	Cobalt oxide
mA	:	Milliampere
eV	:	Electron volt
C_{dl}	:	Double-layer capacitance
ICP-MS	:	Inductively coupled plasma mass spectrometry.
V	:	Volt
Z' (Z_{real})	:	Impedance at X-axis
Z'' (Z_{img})	:	Impedance at Y-axis
$mVdec^{-1}$:	Milivolt per decade
mV	:	Mili volt
AW	:	Acid wash
NSC-AW	:	N/S/Zn-doped porous carbon with acid wash
PB	:	Prussian blue
PBA	:	Prussian blue analogue
MAB	:	Metal-air battery

List of Abbreviations

NiFe- PBA- NG	:	Nickel iron-Prussian blue analogue nanocage
λ	:	Wavelength
Ω	:	Ohm
$^{\circ}\text{C}$:	Degree celsius

List of Figures

Figure No.	Figure Captions	Page No.
Figure 1.1	Overview of (a) Total CO ₂ emission from the consumption of energy (fossil fuels) for the period of 2000-2017 and (b) contribution of RES in the production of electricity at a global level for the year 2017.	3
Figure 1.2	A picture depicting the water-splitting experiment by William Nicholson and Anthony Carlisle.	4
Figure 1.3	Figure showing the cyclic form of OER and ORR in electrolyzer cell, fuel cells and metal-air batteries.	7
Figure 1.4	OER reaction mechanism based on AEM theory. Here * shows the active site (M) of the transition metal cation and I,II,III and IV corresponds to the four elementary steps involved in the reaction.	10
Figure 1.5	Standard free energy plot for the ideal catalyst (a) at zero potential (U=0), equilibrium potential for OER (U=1.23) and (b) at the potential, U = 2.46 V.	12
Figure 1.6	(a) A plot of adsorption energies of HOO* and HO* on metal oxides. Hollow symbols represent the adsorption energy on clean surfaces: perovskites (circle), rutile (triangle), Mn _x O _y (square), anatase (diamond), Co ₃ O ₄ (+). The solid symbols show the adsorption energies on high-coverage surfaces. (b) The volcano relationship between $\Delta G_{O^*} - \Delta G_{HO^*}$ and OER activity for major oxides.	12
Figure 1.7	OER catalytic cycle based on LOM theory. Here, * represents the active site of the catalyst (transition metal cation) and I, II, III and IV are elementary steps.	13
Figure 1.8	(a) A schematic of the composition of a metal-air battery composed of metal as an anode and a porous air electrode as a cathode, and (b) a typical charge-discharge loop for metal-air batteries.	15
Figure 1.9	(a) Schematic representation of the electrolytic cell and fuel cell and, (b) Polarization curves for hydrogen involving	18

List of Figures

	reactions (red curves) and oxygen involving reactions (blue curves).	
Figure 1.10	The plot of the OER activities of the spinels as a function of (a) e_g occupancy of octahedral cation and (b) e occupancy of the tetrahedral cation.	22
Figure 1.11	Graphical representation of MOF and their structural and chemical versatility.	25
Figure 1.12	A roadmap of MOFs materials from the past to present.	26
Figure 1.13	The unit cell structure of Ni-Fe-PBA. Fe^{III} , Ni^{II} , C and N are represented by red, green, purple and black, respectively. Applications of PBAs and their derivatives in various fields.	29
Figure 2.1	Schematic pathways for the preparation of the spinel catalysts.	40
Figure 2.2	Reaction mechanism for the synthesis of Co-MOF.	41
Figure 2.3	Schematic of the synthesis of ZnDTO and NSCs.	43
Figure 2.4	Synthesis of the Ni-Fe-PBA-NC.	45
Figure 2.5	(a) A Photograph of the UV-Vis. spectrophotometer, and (b) a schematic representation of the double-beam spectrophotometer.	46
Figure 2.6	(a) Photograph of the FTIR spectrometer, and (b) the working principle of the Michelson interferometer.	48
Figure 2.7	(a) An Image of the Miniflex 600 X-ray Diffractometer, and (b) a schematic representation of the diffraction of an X-ray beam on a crystallographic material.	49
Figure 2.8	Photograph of the SEM instrument.	51
Figure 2.9	(a) Basic components of SEM (courtesy: Encyclopedia Britannica), and (b) demonstration of the several signals generated by the electron beam sample interaction.	52
Figure 2.10	Image of the XPS instrument.	54
Figure 2.11	(a) Photograph of the BET instrument, and (b) its schematic representation.	56
Figure 2.12	(a) Image of the TGA instrument, and (b) block diagram of its thermo-balance.	57

List of Figures

Figure 2.13	(a) Image of the Autolab NOVA instrument, and (b) electrochemical cell setup.	58
Figure 2.14	A figure of cyclic voltammogram.	59
Figure 2.15	Effect of the scan rate on peak current.	60
Figure 2.16	Impedance curve and its equivalent circuit.	61
Figure 2.17	XRD pattern of commercial RuO ₂ .	62
Figure 2.18	SEM images of RuO ₂ at (a) 1 μm, (b) 200 nm and (c) EDX (carbon present due to the coating).	63
Figure 2.19	(a) N ₂ adsorption-desorption isotherm and (b) pore area distribution plot of RuO ₂ .	63
Figure 3.1	FTIR spectra of NFO-600, NFO-700, NFO-800, NFO-900, CFO-800 and CNFO-800.	66
Figure 3.2	(a) Room temperature powder X-ray diffraction patterns for Co _x Ni _{1-x} Fe ₂ O ₄ spinel ferrites (with x = 0, 0.5 and 1) calcined at 800 °C for 3 hours in N ₂ atmosphere. The Le-Bail fits for (b) CFO, (c) CNFO, and (d) NFO spinel ferrites.	68
Figure 3.3	Combined XPS survey spectra of NFO-800, CFO-800 and CNFO-800.	69
Figure 3.4	XPS profile of (a) Ni 2p (b) Fe 2p, (c) O 1s, and (d) C 1s in NFO-800.	70
Figure 3.5	XPS profile of (a) Co 2p, (b) Fe 2p, (c) O 1s, and (d) C 1s in CFO-800.	71
Figure 3.6	XPS profile of (a) Co 2p, (b) Ni 2p, (c) Fe 2p, (d) O 1s and, (e) C 1s in CNFO-800.	71
Figure 3.7	N ₂ adsorption-desorption isotherms of (a) NFO-800, (b) CFO-800, (c) CNFO-800 and the corresponding NL-DFT pore size distribution (a') NFO-800, (b') CFO-800 and (c') CNFO-800.	73
Figure 3.8	SEM images of (a) NFO-600, (b) NFO-700, (c) NFO-800, (d) NFO-900, (e) CFO-800, and (f) CNFO-800.	74

List of Figures

Figure 3.9	EDS Elemental mapping analysis of underlined area in NFO-600.	75
Figure 3.10	EDS Elemental mapping analysis of underlined area in NFO-700.	75
Figure 3.11	EDS Elemental mapping analysis of underlined area in NFO-800.	76
Figure 3.12	EDS Elemental mapping analysis of underlined area in NFO-900.	76
Figure 3.13	EDS Elemental mapping analysis of underlined area in CFO-800.	77
Figure 3.14	EDS Elemental mapping analysis of underlined area in CNFO-800.	77
Figure 3.15	(a) Liner sweep voltammograms of NFO-600, NFO-700, NFO-800 and NFO-900 and (a') corresponding Tafel plots. (b) Liner sweep voltammograms of NFO-800, CFO-800 and CNFO-800 and (b') corresponding Tafel plots. Liner sweep voltammograms were recorded at a scan rate of 5 mVs ⁻¹ in 0.1 M KOH.	80
Figure 3.16	(a) Electrochemical impedance spectra of NFO-600, NFO-700, NFO-800, and NFO-900 and (b) electrochemical impedance spectra of NFO-800, CFO-800 (inset graph representative equivalent circuit) and NCFO-800.) Impedance was measured at an applied potential of 346 mV of η in 0.1 M KOH solution.	82
Figure 3.17	Linear sweep voltammograms of NFO-800 before and after 500 continuous CV cycles.	83
Figure 4.1	Powder X-Ray diffraction pattern for Anthranilic acid (AA) and Co-MOF.	88

List of Figures

Figure 4.2	UV-Vis. diffuse reflectance spectra measured at room temperature and their corresponding K-M function plot.	90
Figure 4.3	FT-IR spectra of Anthranilic acid and Co-MOF.	91
Figure 4.4	(a) Full survey XPS spectrum of AA and Co-MOF, high-resolution XPS spectrum of (b) C _{1s} , (c) O _{1s} , and (d) N _{1s} in Anthranilic acid (AA).	92
Figure 4.5	The core level deconvoluted spectrum of (a) Co _{2p} , (b) C _{1s} , (c) O _{1s} and (d) N _{1s} in Co-MOF.	93
Figure 4.6	Mass spectra of Co-MOF.	94
Figure 4.7	Optimized structure of Co-MOF and its HOMO-LUMO.	95
Figure 4.8	Williamson-Hall plot corresponding to Co-MOF.	96
Figure 4.9	(a) Schematic representation of the mechanism of reaction and growth process in flower structure of Co-MOF, (b) FE-SEM image, (c) EDX spectrum, and from (d) to (g) elemental mapping of a selected area of Co-MOF.	97
Figure 4.10	Distribution plots for the (a) size of the flower and (b) petals length in Co-MOF.	98
Figure 4.11	(a) N ₂ adsorption-desorption isotherm and (b) pore area distribution plot of Co-MOF.	99
Figure 4.12	(a) LSV polarization curve at 5 mVs ⁻¹ , (b) Tafel slopes, (c) Nyquits plot, (d) double layer capacitance (C _{dl}) calculation at 1.22 V vs RHE of Co-MOF and RuO ₂ in 0.5 M KOH, (e) chronoamperometry of Co-MOF for 15,000 seconds at a static overpotential of 500 mV in 0.5 M KOH and (f) response of OER current before and after stability. The cell configuration (R-reference, C-counter, and W-working electrode) for the chronoamperometry measurement is shown in inset [figure 1.2(e)].	101

List of Figures

Figure 4.13	Cyclic voltammetry (CV) of (a) Co-MOF at varying scan rates from 10 to 100 mV s ⁻¹ .	102
Figure 5.1	FT-IR of (a) DTO, ZnDTO (b) NSC-5, NSC-7, NSC-9, NSC-7AW and (c) Co ₃ O ₄ , Co ₃ O ₄ NSC-7 and Co ₃ O ₄ NSC-7AW.	108
Figure 5.2	Powder XRD of (a) ZnDTO, NSC-7 and NSC-7AW, (b) Co ₃ O ₄ , Co ₃ O ₄ NSC-7 and Co ₃ O ₄ NSC-7AW respectively.	109
Figure 5.3	XPS for ZnDTO corresponding to (a) XPS survey, (b) Zn _{2p} , (c) N _{1s} , (d) S _{2p} (e) C _{1s} and (f) O _{1s} .	110
Figure 5.4	XPS of NSC-7 corresponding to (a) survey spectrum, (b) Zn _{2p} , (c) N _{1s} , (d) S _{2p} and (e) C _{1s} .	111
Figure 5.5	XPS of NSC-7AW corresponding to (a) XPS survey (b) Zn _{2p} , (c) N _{1s} , (d) S _{2p} and (e) C _{1s} .	112
Figure 5.6	XPS spectrum of Co ₃ O ₄ corresponding to (a) survey spectrum, (b) Co _{2p} and (c) O _{1s} .	113
Figure 5.7	XPS of Co ₃ O ₄ NSC-7 corresponding to (a) survey spectrum, (b) Zn _{2p} , (c) Co _{2p} , (d) N _{1s} , (e) S _{2p} and (f) C _{1s} and (g) O _{1s} .	114
Figure 5.8	XPS of Co ₃ O ₄ NSC-7AW corresponding to (a) survey spectrum, (b) Zn _{2p} , (c) Co _{2p} , (d) N _{1s} , (e) S _{2p} , (f) C _{1s} and (g) O _{1s} .	115
Figure 5.9	TGA of DTO, PVP and ZnDTO.	117
Figure 5.10	FE-SEM images of (a) ZnDTO, (b) NSC-7, (c) NSC-7AW, (d) Co ₃ O ₄ , (e) Co ₃ O ₄ NSC-7 and (f) Co ₃ O ₄ NSC-7AW.	118
Figure 5.11	FE-SEM images of (a) NSC-5 and (b) NSC-9.	119
Figure 5.12	N ₂ adsorption-desorption isotherms of (a) NSC-7, (b) NSC-7AW, (c) Co ₃ O ₄ NSC-7 and (d) Co ₃ O ₄ NSC-7AW. The corresponding pore size distribution curves are shown in inset.	120

List of Figures

Figure 5.13	Linear sweep voltammograms of ZnDTO, NSC-5, NSC-7 and NSC-9 at scan rates of 5 mVs ⁻¹ (a') corresponding Tafel slopes, (b) Linear sweep voltammograms of NSC-7, NSC-7AW, Co ₃ O ₄ NSC-7, Co ₃ O ₄ NSC-7AW, Co ₃ O ₄ and RuO ₂ at scan rates of 5 mVs ⁻¹ and (b') corresponding Tafel plots in 0.5 M KOH. Figure (c) and (d) represents the plot of the current density with respect to mass.	128
Figure 5.14	Electrochemical impedance spectra of (a) ZnDTO, NSC-5, NSC-7 and NSC-9 and (b) NSC-7, NSC-7AW, Co ₃ O ₄ NSC-7, Co ₃ O ₄ NSC-7AW, Co ₃ O ₄ and RuO ₂ in 0.5 M KOH.	130
Figure 5.15	EIS fitting of (a) ZnDTO, NSC-5, NSC-7, NSC-9 and NSC-7AW and (b) Co ₃ O ₄ , Co ₃ O ₄ NSC-7 and Co ₃ O ₄ NSC-7AW. Inset of each graph shows their representative electrochemical equivalent circuit.	130
Figure 5.16	(a) Plot of the double layer capacitance (C _{dl}) with respect to scan rates and (b) cyclic stability of Co ₃ O ₄ NSC-7 for 200 CV cycles at 50 mVs ⁻¹ scan rate. The inset figure shows the LSV curve before and after 200 CV cycles.	132
Figure 5.17	(a) Chronoamperometry of Co ₃ O ₄ NSC-7 in 0.5 M KOH for 2 hours and (b) response of LSV current at (I) 0 hour and (II) 2 hours. The inset of the figure (a) shows the cell configuration (R-reference, C-counter, W-working electrode). Continuous O ₂ bubbles are formed on modified Torey paper during the test.	134
Figure 5.18	FE-SEM images of Co ₃ O ₄ NSC-7 (a) before and (b) after chronoamperometry for 7200 seconds in 0.5 M KOH.	134
Figure 6.1	Le Bail Profile Matching & Integrated Intensity Refinement of the XRD patterns corresponding to (a) NiFe-PBA-NC, (b) NiFe-PBA-NG and (c) NiFe oxide.	140
Figure 6.2	FT-IR spectrum of NiFe-PBA-NC, NiFe-PBA-NG and NiFe oxide.	143

List of Figures

Figure 6.3	XPS for NiFe-PBA-NC corresponding to (a) survey, (b) Ni 2p, (c) Fe 2p, (d) C 1s, (e) N 1s and (f) O 1s.	144
Figure 6.4	XPS for NiFe-PBA-NG corresponding to (a) survey, (b) Ni 2p, (c) Fe 2p, (d) C 1s, (e) N 1s and (f) O 1s.	145
Figure 6.5	XPS for NiFe oxide corresponding to (a) survey, (b) Ni 2p, (c) Fe 2p and (d) O 1s.	146
Figure 6.6	TGA of NiFe-PBA-NC.	147
Figure 6.7	HR-SEM image of (a, a') NiFe-PBA-NC, (b, b') NiFe-PBA-NG and (c, c') NiFe oxide.	148
Figure 6.8	Optimization of ammonia solution and time (a) 500 μ L, 1 hour; (b) 1.3 mL, 1 hour; (c) 3.5 mL, 1 hour; (d) 5 mL, 2 hour; (e) 2.6 mL, 5 hour; (f) 500 μ L, 15 hour for nanocage formation from nanocubes.	149
Figure 6.9	N ₂ adsorption-desorption isotherms of (a) NiFe-PBA-NC, (b) NiFe-PBA-NG, (c) NiFe oxide and the corresponding NL-DFT pore size distribution (a') NiFe-PBA-NC, (b') NiFe-PBA-NG, and (c') NiFe oxide.	150
Figure 6.10	(a) LSV, (b) Tafel slopes, (c) Nyquist plots of NiFe-PBA-NC, NiFe-PBA-NG, NiFe oxide and RuO ₂ at scan rates of 5 mVs ⁻¹ in 0.1 M KOH.	152

List of Tables

Table No.	Table Captions	Page No.
Table 1.1	MOFs and MOF based materials for various applications	27
Table 3.1	BET surface area and other parameters of NFO-800, CNFO-800 and CFO-800.	74
Table 3.2	Electrocatalytic impedance parameters of the catalysts.	82
Table 4.1	Structural parameters for optimized Co-MOF.	95
Table 5.1	Atomic percentage of Zn, N and S in catalysts obtained from XPS measurements.	116
Table 5.2	BET parameters of the catalysts.	120
Table 5.3	Contact angle of the catalysts.	122
Table 5.4	Amount of Co and Zn in Co ₃ O ₄ NSC-7 and Co ₃ O ₄ NSC-7AW.	123
Table 5.5	EIS parameters of the catalysts fitted with R(QR) circuit.	131
Table 5.6	EIS parameters of the catalysts fitted with R(QR)(QR)(CR) circuit.	131
Table 5.7	Comparison of OER performance of composite materials derived from MOF and other additives.	135
Table 6.1	Structural parameters for materials.	141
Table 6.2	BET surface area and other parameters of the materials.	151
Table 7.1	Comparison of OER performance of different types of electrode materials.	156-157

Preface

Energy is the foremost factor for the growth of any country and its economic development. In developing countries like India, energy consumption increases at a fast rate due to population growth and development infrastructure. Currently, most of the energy demand is full-filled by coal-based power, which creates pressure on fossil fuels. In 2017, approximately 73.5% of the electricity was produced from the fossil-fuels and the combustion of fossil fuels generates greenhouse gases which affect the environment severely, leading to climate change. This creates a big problem for energy conservation and environmental protection for the next generation. The scientific community worldwide is continuously making efforts to find effective alternatives to these fossil-based fuels. Renewable energy sources (REs) such as solar, wind, water electrolysis (water-splitting) and geothermal energy are clean and environmentally friendly energy sources and integration of these renewable sources in power generation manages the energy requirement up to a certain level. Among the various REs, water-splitting shows great promise in producing green fuel as a hydrogen gas (H_2) and molecular oxygen (O_2) as an oxidant. It is driven by two half-reactions, hydrogen evolution reaction (HER) and oxygen evolution reaction (OER) and fossil fuel consumption is greatly reduced by using H_2 as a fuel carrier because of its high energy density ($120-142 \text{ MJ kg}^{-1}$), which in turn controls the climate change and display a path for sustainable green fuel.

Using H_2 as a fuel effectively is possible when water splits into H_2 and O_2 simultaneously through HER and OER, respectively. Compared to HER, OER is a more complex reaction, and it requires a high overpotential to reach the same current density, which implies that the kinetic barrier of OER is harder to overcome. Besides being requisite in water-splitting as a half-reaction, OER is also significant for generating molecular oxygen (O_2). Oxygen is a vital component for living and in the corona-pandemic, we learned about the importance of oxygen. Besides from this, it has multifaceted utilizations in

Preface

various industries. In energy conversion and storage devices such as fuel cells and metal-air batteries, OER plays a vital role in electrochemical conversion cycles between renewable electricity and chemical fuels via the generation of pure oxygen in a short period. Therefore, accelerating the development of OER is urgent for close-looped clean energy infrastructure and overcoming the shortage of oxygen due to growing pollution.

Ru and Ir-based catalysts are considered as state-of-the-art OER electrocatalysts but due to the high cost and element scarcity are not sustainable choices. At the same time the electrochemical stability of the oxides of these materials (RuO_2 and IrO_2 transform into $[(\text{Ru}^{8+})\text{O}_4]$ and $[(\text{Ir}^{6+})\text{O}_3]$, respectively in the aqueous solution) hinders their applications at large-scale. Transition metal oxides, with various physical and electronic properties, are considered promising low-cost alternatives. In this, spinel-type oxides with significant performance have been extensively investigated as OER electrocatalysts. On the other hand, metal-organic frameworks have emerged as an important class of functional material due to their well-defined structural designs, high surface area, porosity, excellent thermal and mechanical stability and diverse chemical functionalities.

The thesis entitled “Metal-organic framework and nanomaterials for oxygen evolution reaction” encompasses the synthesis of spinel materials; nickel ferrite (NFO), Co-doped nickel ferrite (CFO and CNFO) and metal-organic frameworks (MOFs), e.g. Co-MOF (cobalt metal-organic framework), ZnDTO (zincdithiooxamide) MOF and Ni-Fe PBA-NC (nickel-iron Prussian blue analogue nanocube) for OER. Further, MOFs are used as a precursor to derive heteroatom-doped porous carbon, nanocomposite and various nanostructures to enhance the OER activity of MOFs. Based on the findings the thesis has been divided into seven chapters.

Preface

Chapter 1 is the introductory part which describe about the water splitting, its thermodynamic feasibility at different pH, OER in water splitting, mechanism of OER in different pH and its mechanistic approach, importance of OER in other fields like metal-air batteries and fuel cells, besides the water splitting, emerging electrocatalysts for OER such as spinels, perovskites, metal oxides, LDH (layered double hydroxide) and MOFs. This chapter also deals with the evaluating kinetic parameters for OER activity of the catalysts viz. selection of electrolyte, onset/ overpotential, Tafel slope, exchange current density, ECSA (electroactive surface area) and stability.

Chapter 2 is the experimental and instrumentation part. It covers the details of the chemicals, synthesis of the electrocatalysts, nickel ferrite (NFO), Co-doped nickel ferrite (CFO and CNFO), Co-MOF, ZnDTO MOF, N/S/Zn doped porous carbon (NSC), nanocomposite of Co_3O_4 and NSC, Ni-Fe PBA nanocube, Ni-Fe PBA nanocage and Ni-Fe mixed oxide which are used in the further chapters and their characterizations with different characterization techniques such as UV-Vis. (ultraviolet-visible), XRD (X-Ray Diffraction technique), FT-IR (Fourier transfer infrared), SEM (Scanning Electron Microscopy) etc. Further, electrode preparation and electrochemical measurement methods viz. CV (cyclic voltammetry), LSV (linear sweep voltammetry), EIS (Electrochemical impedance spectroscopy) and CA (chronoamperometry) are described to analyse the OER performance of the catalyst materials. Then the OER performance of the catalysts is compared with commercially available RuO_2 .

Chapter 3 In this chapter spinel materials; nickel ferrite (NFO) and Co-doped nickel ferrite (CFO and CNFO) are used for OER analysis. Sol-gel method is used for the synthesis of nickel ferrite and for the first time Co-doped nickel ferrite. OER performance of NFO, CFO and CNFO are checked by LSV and EIS. For the stability of the best

Preface

catalyst, 200 CV cycles are recorded and then LSV is performed and compared with before 200 CV cycles.

Chapter 4 In this work, we reported a beautiful rose-like structured Co-MOF, comprising petal-like sheets, as an active material to modify the commercial glassy carbon electrode (GCE) for enhanced OER performance. The Co-MOF is synthesised by a facile precipitation method using cobalt salt (Co^{2+}) and Anthranilic acid (AA). Detailed characterization techniques thoroughly explained the complexation of Co^{2+} with AA and the flower morphology of Co-MOF. Along with that, the optimised structure of Co-MOF and HOMO-LUMO is analysed by DFT. Further, the OER activity of the Co-MOF is investigated by LSV, Tafel slope, and compared with commercially available RuO_2 and for stability measurement, CA is employed for 10800 seconds at a static overpotential of 500 mV.

Chapter 5 In this chapter, Co_3O_4 nanoparticles embedded in N/S/Zn- doped porous carbon matrices is utilized as active materials to modify the commercial glassy carbon electrode (GCE) for enhanced and highly stable oxygen evolution reaction (OER). Firstly, a metal-organic framework (spherical ZnDTO, synthesized by the complexation of Zn-salts and dithiooxamide (DTO) ligand) is used. Then, N/S doped porous carbons (NSC) are derived from ZnDTO MOF by carbonizing them at different temperatures and to investigate the role of Zn on the catalytic performance of the materials, the thermally optimized carbon matrix is treated with a suitable acid. Further to enhance the OER activity, nanocomposite is formed with Co_3O_4 nanoparticles and these carbon matrixes. All the as-synthesized materials have been well-characterized by various tools for their structural and morphological associations.

Preface

Chapter 6 explores another class of MOF, Prussian blue analogue (PBA) compounds as an OER electrocatalyst. Ni-Fe PBA nanocubes are synthesised by a precipitation method and then via a facile chemical etching process (with ammonia solution), nanocubes are transformed into nanocages. A control etching process is developed in which etching occurs preferentially on the corners constructing the hollow cubes. Further, on annealing in air, the nanocubes are converted into NiFe-oxides, porous cubes. Both the nanostructures generated from nanocubes reveals different chemical composition retaining cubic morphology. XRD refinement, FT-IR, XPS and FE-SEM well-confirmed the conversion of the nanocubes to nanocage and oxide. Then, these materials are employed for OER analysis in which NiFe oxide shows enhanced performance.

Chapter 7 includes the conclusive remarks and future prospects of the thesis.

CONTENTS

	Page No.
List of Figures	i-viii
List of Tables	ix
List of Abbreviations/ Symbols	x-xii
Preface	xiii-xvii
Chapter – 1 Introduction and Literature survey	1-37
1.1 General Introduction	1
1.2 Water splitting	2
1.3 Oxygen evolution reaction (OER)	6
1.4 Importance of OER in other fields	14
1.5 Emerging electrocatalysts for OER	20
1.6 Evaluating parameters for OER activity	29
1.7 Scope of the work and objective of the thesis	35
Chapter-2 Experimental and instrumentations	38-63
2.1 Experimental	38
2.2 Characterization techniques	45
2.3 Characterizations of commercially available RuO ₂	62
Chapter-3 Studies on spinel oxides-based electrocatalysts for oxygen evolution reaction	64-84
3.1 Introduction	64
3.2 Results and discussions	65
3.3 Conclusions	84
Chapter 4 Co-MOF derived from Co-salt and Anthranilic acid for enhanced oxygen evolution reaction	85-102
4.1 Introduction	85
4.2 Results and discussions	88
4.3 Conclusions	102

CONTENTS

Chapter-5 Enhanced OER properties of nanocomposites of Co₃O₄ and MOF derived N/S/Zn doped porous carbon	103-136
5.1 Introduction	103
5.2 Results and discussions	107
5.3 Conclusions	135
Chapter-6 Engineered Ni-Fe Prussian-blue-analogue nanocube and their conversion into Nano cage and mixed oxide for oxygen evolution reaction	137-153
6.1 Introduction	137
6.2 Results and discussions	139
6.3 Conclusions	152
Chapter-7 Summary and future outlook	154-158
References	159-182
List of Publications	183-184
List of Conferences	185